Nano Energy 84 (2021) 105874

Contents lists available at ScienceDirect

Nano Energy

journal homepage: http://www.elsevier.com/locate/nanoen

High symmetry nano-photonic quasi-crystals providing novel light management in silicon solar cells

Thomas M. Mercier [a,*,1], Tasmiat Rahman [a], Chirenjeevi Krishnan [a], Edris Khorani [a], Peter J. Shaw [a], Michael E. Pollard [c], Stuart A. Boden [a], Pavlos G. Lagoudakis [b], Martin D. B. Charlton [a]

[a] Electronics and Computer Science, University of Southampton, Southampton, United Kingdom
[b] Physics and Astronomy, University of Southampton, Southampton, United Kingdom
[c] School of Photovoltaic and Renewable Energy Engineering, University of New South Wales, Kensington, NSW 2052, Australia

ARTICLE INFO

Keywords:
Photonic crystal
Silicon
Solar cell
IBC
Nanofabrication
FDTD

ABSTRACT

Reduction of surface reflection loss is crucial for high efficiency next generation Si solar cells. Surface texturing provides a viable method to reduce loss over the full solar bandwidth. Previous studies have concentrated on simple moth-eye silicon pillar arrays protruding from the surface. Using FDTD simulation methods, we undertake a systematic investigation into performance benefits provided by complex semi-random photonic quasi-crystal surface patterning methodologies whereby arrays of air holes are etched deep into the solar cell surface. In contrast to other studies we carefully investigate the effect of lattice symmetry, systematically comparing performance of simple 6-fold symmetric triangular photonic crystal patterning to 12 fold symmetry photonic quasicrystal patterning and infinitely symmetric 2D Fibonacci patterning. We optimize key geometric parameters such as lattice pitch, hole size and etch depth to maximize optical performance for each lattice type. 12 fold photonic quasi crystal lattice is found to provide best overall anti-reflectance performance providing a solar-corrected average reflectance of 8.3% for a hole depth of 1.5 μm and 300 nm diameter, in comparison to 36.4% for a bare silicon solar cell surface. Practical feasibility of the optimal designs is demonstrated by fabrication of physical prototypes consisting of arrays of nm scale air-holes etched into the surface of a silicon slab fabricated Using e-beam lithography and ICP/RIE etching. FDTD Simulation methodology is validated by convergence studies as well as comparison to optical measurements on these fabricated devices. Furthermore, in contrast to previous studies we provide an in depth analysis of the physical mechanisms responsible for reduction in surface reflection, determining the parameter space where conventional Gaussian optical processes such as effective refractive index, refraction and Fresnel reflection dominate, vs parameter space where sub wavelength photonic crystal scattering effects play the main role. We finish up with an analysis of electrical performance for the optimal designs to further validate real world performance. Taking electrical performance into account we determine that infinite-symmetry 2D Fibonacci patterning far outperforms lower symmetry 12 fold and triangular arrangement. We believe that this is the first in depth investigation into 2D Fibonacci patterning in silicon solar cells.

1. Introduction – state of the art and context

Photovoltaic (PV) technologies have shown great promise in meeting ever increasing energy demands whilst avoiding environmental detriment associated with non-renewable alternatives. Si based PV is currently the dominant technology in the solar market (> 90%) [1] due to the natural abundance of Si, well established supply chains and robust fabrication processes. Over the last decade Si PV has provided substantial gain in efficiency and cost effectiveness [1–3]. In order to drive performance-to-cost ratio higher and improve power conversion efficiencies (PCE) significantly further, it becomes necessary to carefully optimize photon management [4,5].

* Corresponding author.
E-mail addresses: t.m.mercier@soton.ac.uk, pvwork13@gmail.com (T.M. Mercier).
[1] Present address: School of Electronics & Computer Science, University of Southampton, University Road, Southampton SO17 1BJ, United Kingdom.

https://doi.org/10.1016/j.nanoen.2021.105874
Received 25 November 2020; Received in revised form 22 January 2021; Accepted 8 February 2021
Available online 11 February 2021

Interdigitated back contact (IBC) cell architecture is one of the most promising emerging Si PV technologies. IBC avoids optical losses associated with front contact shading by eliminating the front contact fingers entirely. It also lends itself well to front surface nano-structuring since no doping of the front surface is required.

Minimization of surface reflectance is one of the most important requirements for efficient PV devices [6]. Si solar cells with no anti-reflectance (AR) measures reflect an average of 40% incident light back into the surrounding medium [7]. The current solution is inclusion of a single layer SiN_x or SiO_2, AR coating (SLAC) which reduces reflectance via destructive interference between waves reflected at the layer surfaces [8–10]. AR coatings can also be devised to serve as multi-functional layers in novel cell architectures that target a reduction in the fabrication cost of Si cells [11]. However, SLAC is only effective over limited solar bandwidth and perfect perpendicular light incidence. SLAC is therefore inefficient for diffuse light harvesting as required on a cloudy or hazy day.

These limitations have led researchers to investigate surface nano-texturing as an alternative, providing the exciting possibility to simultaneously reduce reflection over very wide wavelength range and increase light trapping for large incidence angle range. Current state of the art for surface structure enhanced light trapping in monocrystalline Si PV utilizes micron scale pyramidal pits formed via alkaline etching [6, 12,13]. Further reductions in reflectance can be achieved through combining micro-texturing with AR coatings [14].

Heterogenous 'black silicon' nano-texturing provides a good alternative [15] and can achieve very low reflectance values across a broad range of incident wavelengths due to reduced refractive index associated with the mesoporous structure and dense optical scattering within the material. Subwavelength 'top down' surface etched structures have also been shown to yield reflectance values below 2% across the visible spectrum [16]. Although these methods provide large reduction in reflection loss, they present new challenges due to requirement for good surface passivation to mitigate increased charge carrier recombination at the exposed silicon surfaces [17]. These structures generally work via effective refractive index due to the ratio of air to Si.

Photonic crystals (PhCs) present a promising alternative for light management in Si [18]. PhCs have been shown to be suitable for multiple uses in waveguide applications where light propagates parallel to the plane of the periodicity, and are now utilized in data transceivers for optical networking [19–21]. In these applications they provide precise control over in-plane light propagation and scattering. They have also been incorporated directly into the epi-structures of LEDs where they provide benefit of beam shaping along with substantial improvement in light extraction efficiency [22–27]. In this case light is incident perpendicular to the plane of the structuring.

PhCs have also been incorporated into thin film Si PV devices in an attempt to improve absorption, particularly at longer wavelengths, achieving efficiency improvement of 26% [28]. Arrays of protruding nano-pillars arranged in a 2D hexagonal lattice, have been shown to reduce reflectance to below 10% over the visible spectrum for near-normal light incidence [29]. For the tapered rod structures the reflectance reduction works similarly to moth eye texturing, where the light sees a gradually changing refractive index [30,31].

1.1. Summary of this paper

In this paper we undertake an in-depth analysis of the benefits of etching high symmetry photonic quasi- crystal structures onto the top surface of silicon solar cells as opposed to simple low symmetry triangular lattice PhCs and moth-eye lattices used to date.

Using the established FDTD numerical modeling [6,32] we systematically investigate influence of lattice symmetry in reducing surface reflection over the full solar spectrum, and determine that high symmetry Photonic Quasi-Crystal (PQC) lattices provide exceptional reflection reduction far beyond that possible with standard photonic crystal patterning. PQCs are non-natural lattice arrangements which exhibit short range disorder, and long-range periodicity. Hence, they can be considered semi-random patterns [33–35].

By performing extensive pitch/fill fraction (FF)/hole depth parameter scans, we derive optimized designs for three example lattice types (6 fold triangular photonic crystal, 12 fold symmetric random Stampfli inflated PQC, infinite symmetry 2D Fibonacci lattice PQC) [36]. Due to its resemblance to the head of the sunflower, the 2D Fibonacci lattice PQC is commonly referred to as the sunflower PQC and we will use this term throughout this work [37]. We compare optimal design performance across lattice types, and compare usable design window for robust fabrication.

In order to validate the simulation predications, we fabricate a set of example prototype devices by e-beam lithography and reactive Ion etching, and compare measured broadband reflectance against simulation results for the fabricated structures. The details of the fabrication are described in the methods section. Through simulation convergence testing, we demonstrate that quasi periodic structures can be accurately modeled using a large periodically bounded simulation area.

By comparing PhC/PQC results against an equivalent effective index medium model we are able to provide a detailed insight into the underlying physical mechanisms causing reduced reflectance, and determine the design parameter window where conventional Gaussian optics (refraction, reflection, effective index medium theory) are applicable vs parameter space where nano-scale photonic crystal scattering is applicable. Periodic refractive index modulation provided by the PQC gives rise to a large number of photon-dispersion bands (similar to electron dispersion bands in semiconductor materials) each of which provides a scattering mechanism to couple photons incident onto the surface to 'trapped modes' inside such structures [38]. We show that PQC patterning provides significant reduction in surface reflection over a far larger pitch-FF parameter space/design window due to suppression of Fabry Perot resonances associated with conventional SLAC and low symmetry photonic crystal lattices. We attribute improved scattering to increased density of optical sates available in PQC lattices compared to low symmetry photonic crystal lattices.

Although surface structuring provides a means to radically reduce surface reflection, increased surface area associated with the etched holes could potentially cause degradation of the electrical performance due to increased surface recombination at the surfaces of the etched structures. To mitigate this, we analyze and cross compare electrical performance for optimal designs for each lattice type.

Overall, we demonstrate that PQC surface nano-structuring can achieve broad spectrum reflectance reduction with weighted average reflectance values of 9.2% with no detriment to electrical performance. Furthermore, we give evidence for this reduction of reflectance being the result of PhC effects rather than a simple effective medium as is the case for random texturing. The higher symmetry lattice types are shown to be much more effective in producing a smooth and broad decrease in the reflectance spectra (effective average reflectance (EAR) 12.5% for triangular, 9.2% for 12 fold and 10.1% for sunflower for depth of 1 μm) while keeping the additional surface area at a minimum.

2. Methods

2.1. Simulation setup

FDTD simulation method provides an accurate way to model interactions between light and nano-structures on the same order of magnitude as the wavelength [39–41]. Lumerical's FDTD solutions package was used for all FDTD simulations [42]. Starting with a Si substrate, periodically arranged cylinders with a refractive index of 1 (representing the air holes) are superimposed with the top surface. For the triangular lattice, a simple unit cell with periodic boundary conditions in the x and y directions and perfectly matched layer (PML) boundary in the z direction were used to represent the entire structure,

as is shown in Fig. 1a and b.

Due to the quasi periodic nature of the PQC, no simple unit cell can be used to extrapolate to the behavior of the full crystal symmetry. Since the structures investigated here are limited to a lattice pitch of 800 nm, this was taken into account by using a very large simulation domain of 6 by 6 μm, as can be seen in Fig. 1c and d for the 12 fold and sunflower lattice types. Convergence tests showed that this domain size is sufficient to achieve accurate results. A MATLAB script was used to generate a set of coordinates at which the cylinders were to be placed. The 12 fold lattice is generated by iteration of the Stampfli inflation rule [43]; while the sunflower type PQC is based on a generative spiral and is closely related to the Fibonacci sequence [44]. This set was imported into the FDTD solutions package and a cylinder of a chosen length and diameter was added to each point. A plane wave source of a wavelength range between 300 and 1100 nm with polarization in the x direction was used as a normal incident light source.

Field and power monitors were placed behind and parallel to the plane wave source in order to measure the reflected power as a function of incident wavelength in steps of 1 nm. This arrangement ensures only power reflected from the top surface is detected by the monitor.

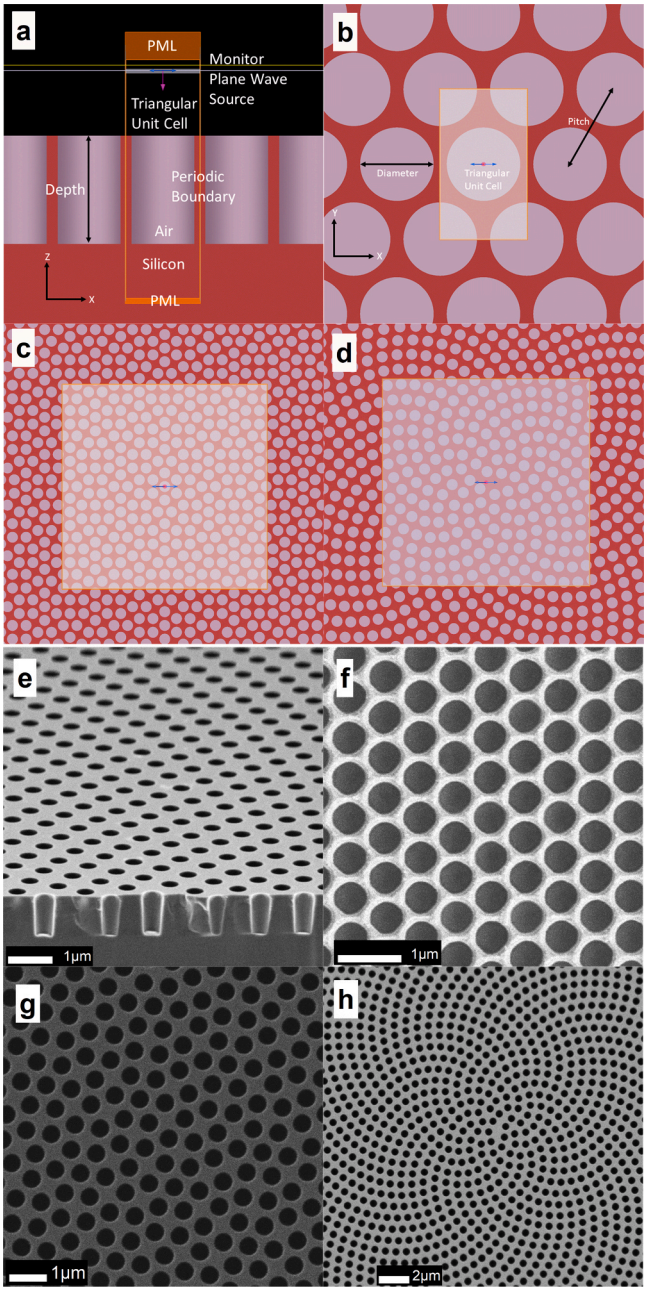

Fig. 1. Overview of lattice types showing both simulated and fabricated structures: (a) Simulation setup XZ cross-section of the triangular lattice type structure. (b) Top view of triangular lattice type structure. (c) Top view with indicated simulation region for 12 fold lattice type structure. (d) Top view with indicated simulation region for sunflower lattice type structure. (e) Cross-sectional SEM image of fabricated sample of sunflower lattice type structure. (f) Top view SEM image of triangular lattice type. (g) Top view SEM image of 12 fold lattice type. (h) Top view SEM image of sunflower lattice type.

2.2. Air fill fraction for PQC lattices

In order to investigate the effects that the details of the PQC geometry have on the amount of light reflected from the structure, the parameters that define the PQC were varied. The main parameters of interest are center to center distance between neighboring holes, (lattice pitch), diameter and the length of the cylinder representing the etched air hole in the Si substrate. Air FF is conventionally given by fractional unit cell area surface occupied by the holes, and is consequently dependent on pitch and hole diameter. The triangular PhC lattice is depicted in Fig. 1b and has a simple FF given by:

$$FF_{Tri} = \frac{2\pi * \left(\frac{d}{2}\right)^2}{\sqrt{3} * p^2} \quad (1)$$

where d is the cylinder diameter and p lattice pitch.

Due to their inherent semi-random nature, PQCs lack a true unit cell. A numerical FF function was instead determined by plotting a high resolution image of filled circles on a blank background with accurately scaled dimensions mimicking the PQC layout. We then find the sum-total number of black image pixels and calculate the ratio to total area image pixel count. This methodology was repeated for a wide range of diameter to pitch ratios and the results fitted with a quadratic polynomial, to yield the following analytical formulas for 12 fold PQC and sunflower lattice types:

$$FF_{12f} = 82.56 * \left(\frac{d}{p}\right)^2 + 0.993 * \left(\frac{d}{p}\right) - 0.103 \quad (2)$$

$$FF_{Sun} = 70.365 * \left(\frac{d}{p}\right)^2 - 0.36 * \left(\frac{d}{p}\right) + 0.071 \quad (3)$$

The effect of lattice pitch, hole diameter and hole depth on spectral reflectivity were investigated. In the simulation setup the plane wave source was placed 600 nm above the top surface of the structure. The mesh type was set to auto non-uniform with the accuracy set to 3 and the minimum mesh step set to 1 nm. In addition to this a substrate mesh with a grid step size of 10 nm was placed in the bulk of the substrate and a mesh with an xy stepsize of 8 nm and a z stepsize of 5 nm was placed to cover the volume taken up by the patterned Si to optimize computing time while maintaining accuracy. These mesh settings were determined by performing convergence tests with decreasing mesh stepsizes. In both the positive and negative z direction a stretched coordinate PML was used while the boundary conditions for the x and y directions were set to periodic.

To gain physical insight into how the photonic crystal structuring differs from a simple effective index layer, the same simulation setup was used, and the part of the substrate that would be penetrated by the PhC holes was replaced with a uniform layer with a refractive index defined by the volume average effective refractive index based on the FF of the corresponding photonic crystal layer [45].

Due to the overall size of the simulation the actual computation was performed by a high performance computing cluster with the highest RAM requirement being 240 gigabytes.

2.3. EAR metric for performance comparison

Broadband reflectivity R for normal incident light, was evaluated by scanning wavelength from 300 to 1100 nm in the simulation tool, then calculating *EAR*. *EAR* was calculated by weighing measured reflectance values R for each wavelength with AM1.5 sun spectrum intensity F, as shown in Eq. (4) [46].

$$EAR = \frac{\int_{\lambda_1}^{\lambda_2} F(\lambda)*R(\lambda)d\lambda}{\int_{\lambda_1}^{\lambda_2} F(\lambda)d\lambda} \quad (4)$$

EAR provides a convenient single figure of merit to judge solar cell performance over the entire solar spectrum.

2.4. Electrical simulations in Quokka

To evaluate the results of the optical simulations in a device context, the reflectance spectra for the best performing geometries were used in a Quokka simulation [47,48]. Quokka is a MATLAB-based tool developed for the simulation of silicon solar cell devices in three dimensions and employs the general semiconductor carrier transport model to solve for the steady-state electrical characteristics of such devices. This is used to define an IBC silicon solar cell using the experimental parameters taken from the 24.4% PCE IBC made at Australian National University [13,49,50]. The simulation calculates a current density (J) for a range of voltages (V) giving a J-V curve that allows the short circuit current density (J_{SC}), open circuit voltage (V_{OC}) and efficiency to be calculated.

To account for the differences in total surface area due to the designs, the surface recombination velocity (SRV) of the top surface was scaled by a correction factor based on sidewall area of each design. This area can be calculated by multiplying the total circumference of the holes in a fixed substrate area by the depth of the holes. This sidewall area will depend on both the lattice pitch, lattice type and hole diameter. Adding this sidewall area to the surface area of the unpatterned surface and setting it in relation to this unpatterned surface area, results in a correction factor that can be used to scale the base SRV of 2 cm/s. This was done to account for the fact that the additional sidewall area introduces additional recombination sites. In a real device the surface of the Si would have to be passivated using an appropriate passivation layer. Since good passivation levels can be achieved with very thin layers, such as 10 nm of Al_2O_3, this would not have a large effect on how the light interacts with the structuring and was therefore not included in the optical simulation [51].

2.5. Fabrication

In order to demonstrate the feasibility of the proposed nanostructures and to support the validity of the simulation results, comparison samples were fabricated. An overview of the fabrication steps is depicted in Fig. 2. A polished Si wafer of 650 μm thickness was used as the substrate for the fabrication. First a 300 nm SiO_2 hard mask was deposited using a Leybold HELIOS reactive sputtering system. The desired pattern was then defined in a 400 nm thick ZEP500 positive resist using a 100 kV JEOL 9300 E-Beam lithography system. E-Beam lithography was chosen for the patterning of this fabrication process, because it enabled the definition of multiple different lattice types and geometries on the same wafer. Furthermore, small sizes of the holes ($<$ 500 nm) required very precise lithography. After development the pattern was transferred to the hard mask using an Oxford Instruments Reactive Ion Etching (RIE) tool. A highly selective SiO_2 etching recipe based on CHF_3 gas was used for the hard mask etch. The etching was carried out in a cyclical fashion with N_2 cooling steps in-between etching steps to prevent burning of the resist. This was followed by etching the pattern into the bulk Si substrate by using an Oxford Instruments Inductively Coupled Plasma (ICP) RIE tool. For this transfer step a Cl based etching recipe was used to achieve fast etching with reasonably

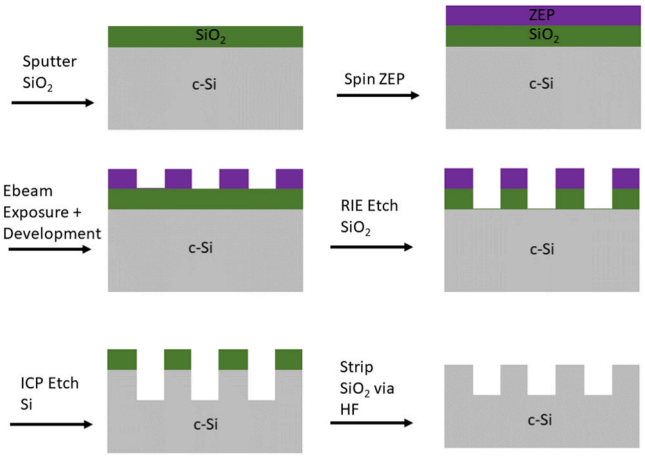

Fig. 2. Fabrication process flow for PhC/PQC nanostructures in Si.

straight sidewalls. The ICP etcher used an ICP power of 750 W and the table was kept at 20 C. The remaining hard mask was then removed via buffered HF wet etching. Scanning Electron Microscopy (SEM) images of the results of the fabrication were taken using a Zeiss NVision 40 Focused Ion Beam system with the cross-sectional images being of a cleaved sample. The cross-sectional image can be seen in Fig. 1e.

2.6. Accurate simulation of fabricated structures

In order to ensure that realistic device dimensions were used in the simulations, sample devices were fabricated and dimensions measured by SEM. Hence Fig. 1e–h shows top and cross-sectional view SEM images of fabricated samples for each lattice types. From the SEM images it can be seen that all the PhC and PQC holes are well defined and uniformly etched. From the cross-sectional SEM image it is apparent that there is a slight narrowing of the hole diameter with increasing depth.

2.7. Measurement

Optical performance of fabricated devices was measured using a Bentham PVE 300 system utilizing a Xenon and Halogen source with the incoming beam at 8 degrees from the normal of the sample surface. The measurement is conducted using an integrating sphere setup to collect all reflected light (both specular and diffuse) over 2π SR solid angle.

The measurement system, as depicted in Fig. 3, utilizes two light sources, one Xenon and one Halogen source to produce a wide range of wavelengths. This light then enters a monochromator where a grating reflects the different wavelengths, so that only a single wavelength hits a slit leading to the optics of the system. The optics then focus the light into an integrating sphere. The sample is mounted at the back of the integrating sphere with the monochromatic light being incident on the sample at 8 degrees. The monochromator sweeps the incident

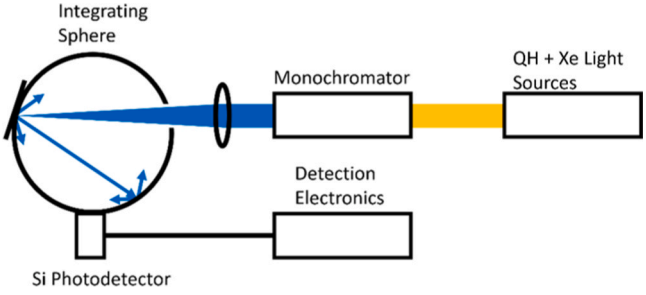

Fig. 3. PVE300 reflectance measurement system used to measure reflectance of fabricated samples.

wavelength from 300 to 1100 nm in steps of 5–10 nm. A Si based detector then produces a current due to the light incident upon its surface. Using a comparison measurement from a Bentham calibrated diffuse reference sample the measurement electronics then convert this current into a reflectance value.

3. Results and discussion

3.1. Simulation convergence testing

PQCs are highly unusual in possessing long range order but short-

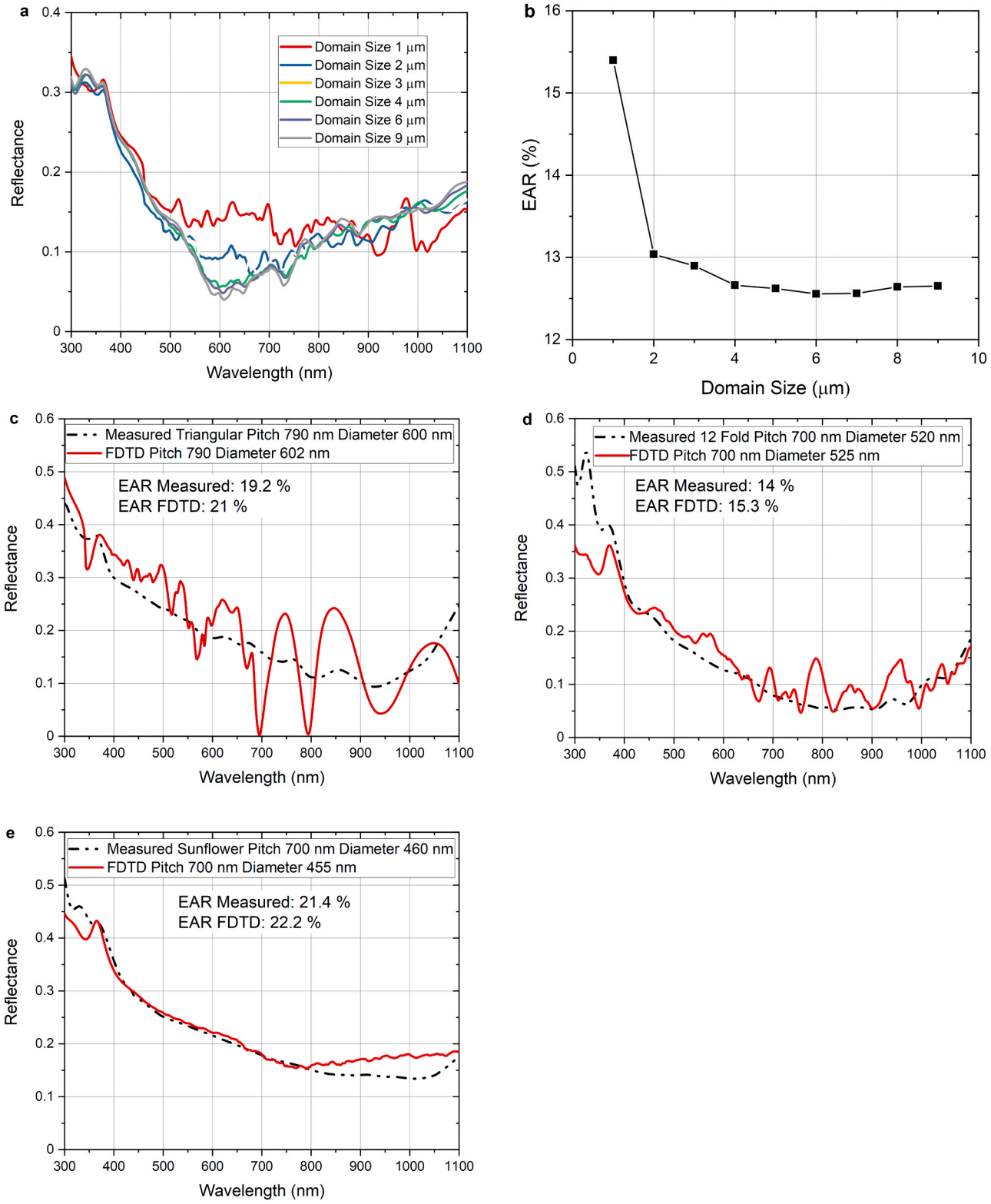

Fig. 4. Validation of FDTD simulation setup. (a,b) Domain convergence for sunflower PQC structures for lattice pitch of 500 nm with a FF of 54% and hole depth of 700 nm with (a) showing individual spectra and (b) showing EAR values for domain sizes. (c–e) FDTD simulation results compared to measurement for (c) triangular, (d) 12 fold and (e) sunflower lattice type.

range disorder, and so can be classed as semi random structures [33]. Although this attribute is highly useful in applications (and is exploited here), it makes accurate simulation extremely challenging since the simulation domain size must be large enough to include several repetitions on the scale of the long-range order. As the level of symmetry increases this distance increases. To put this in context of conventional semiconductor solid state theory for defect lattices, the simulation domain must extend over the lattice 'super-cell' size, hence the need to perform convergence tests.

To validate FDTD simulation accuracy, reflectance vs wavelength was plotted as function of increasing simulation domain size (Fig. 4a). Domain size < 3 by 3 μm^2 is found to overestimate reflectance for wavelengths > 500 nm whilst change in reflectance become negligible for domain sizes > 4 by 4 μm^2 as further validated by Fig. 4b EAR plot. Both sunflower and 12 fold PQC lattice types are well converged at a domain size of 6 by 6 μm^2 hence this was chosen for all subsequent simulations. Additional domain space would only add to simulation time without improving accuracy.

3.2. Comparison between experiment and simulation

In order to demonstrate validity and give confidence in accuracy of the simulation methods which underpin the key findings of this paper, we first present a comparison between simulated and experimental reflectance measurement for a set of fabricated devices with each lattice type.

Fig. 4c shows simulated and measured reflectance spectrum for a triangular lattice PhC patterned solar cell. The simulation follows the general trend of the measured reflection spectrum, but has highly pronounced dips at 700, 800 and 950 nm. These dips are also present in the experimental measurement but weakly pronounced. Difference in extinction ratio for these features between measurement and simulation is due to the fact that the simulation models directional incidence and reflection of a coherent light source, whereas the experimental integrating sphere measurement system measures both directly reflected and diffuse light scattered at all angles from an incoherent light source, and so blurs the fine features due to lack of angular resolution. Furthermore, difference in the wavelength step size used in the simulation (1 nm) and limited step size available from the experimental measurement (5–10 nm) further reduces resolution of the measurement. Nonetheless the features are clearly present in the measurement at equivalent wavelengths albeit with reduced modulation amplitude. Computing the EAR values for the simulated and measured results shows a 1.8% point difference.

Fig. 4d shows simulated and measured reflectance spectra for a 12 fold symmetric PQC device. Simulation and measurement plots are far more closely matched compared to the triangular lattice, with a small deviation at UV wavelengths below 400 nm. The EAR values only show a 1.3% point difference.

Fig. 4e compares simulation and measurement for the sunflower lattice device. In this case we find a near perfect match over wavelength range 350–800 nm with a small deviation at longer wavelengths.

We note that the deviation occurs at a wavelength close to the lattice pitch. Over these short length scales, regions of the lattice appear quite periodic and so it is likely diffraction will occur due to interference between light reflected from ensembles of neighboring holes. Over the longer length scale however the positional placement of the holes deviates slightly, and the lattice becomes more random. Noting that the experiment averages over a very large lattice area, diffraction effects would be expected to become visible only in the simulation if a relatively small area of lattice is incorporated in the simulation.

Due to its near-infinite symmetry and subsequent longer periodic length scales, the sunflower lattice is most sensitive to simulation domain size in comparison to 12 fold lattice. Hence we attribute the deviation between experiment and simulation at longer wavelengths to the limited domain size used in the simulation. Domain size could not be increased further due to the limitations of the available computational resources.

The EAR values show a difference of 0.8% points, clearly showing that the sunflower gave the closest match between simulation and experiment.

Overall these measurements provide evidence that the simulation setup is reliable in its ability to accurately predict spectral reflectance of PQC structures, and reveals the limitation of the conventional integrating sphere measurement system in tracking fine angular diffractive features.

The smooth PQC reflectance spectra observed in Fig. 4 suggests that angular diffraction efficiency decreases as lattice symmetry increases from 6 fold (triangular) to 12 fold PQC and infinity (sunflower), making light scattering more homogenous.

3.3. Optimization of PQC design parameters

Having established validity of the simulation methods we next determine optimal PQC designs to minimize EAR for each lattice type. We start by investigating effect of PQC pitch and FF and compare relative merits of each.

Fig. 5 shows EAR encoded as color map, as function of lattice pitch and FF, with an air cylinder etch depth of 1000 nm for all cases. Maximum achievable FF is limited by the packing density of the holes for each lattice type and reduces with lattice symmetry according to Eqs. (1–3) presented in the methods section, hence non-physical regions of the graphs are crossed out. Blue areas denote low reflectance (desirable) and red high reflectance (to be avoided).

It can be seen that the behavior of all three lattices is very similar in terms of overall trend. We observe that reflectance decreases significantly for FF $> 50\%$ over lattice pitch range 400–700 nm (blue areas of color map). However, lattice pitch > 700 nm gives higher reflectance. It is particularly noticeable that FFs $< 30\%$ yield significantly worse reflectance performance (red areas) than higher FF.

Looking more closely at the triangular lattice plot Fig. 5a, we observe structured features in the blue shaded regions, corresponding to sharp PhC dispersion modes. These features are not evident in the plots for the PQC lattices (Fig. 5b,c) due to the low density of optical states (DOS) provided by the 6-fold symmetric triangular lattice. DOS actually increases with lattice symmetry due to the fact that PQCs provide a continuum of dispersion bands as opposed to sparse discrete bands for the triangular lattice, hence 12 fold PQC and infinity sunflower do not exhibit dispersion features in the EAR plots [52].

More significantly, we find that the triangular lattice cannot achieve the same low level of EAR as the PQC lattices (blue color scale). The triangular lattice type achieved a minimum EAR of 12.5%, while the 12 fold lattice achieved 9.2% and the sunflower gave a minimum of 10.1%. With regard to design parameter space, we conclude that FF must be carefully controlled in order to minimize EAR, whereas pitch precision is less important. To give context to these performance numbers we present the EAR values of typical AR approaches in Table 1. As can be seen the PQC structures outperform both SLAC and pyramid based AR schemes unless the pyramids are combined with a SLAC. It should be pointed out that combining a SLAC with structuring could also improve the EAR performance of the PQCs.

For the design of a realistic device the fabrication restrictions and process repeatability need to be considered, hence a realistic window of parameters for these structures would leave 20–50 nm between adjacent holes, which somewhat limits the achievable FF (around 78% for triangular, 75% for 12 fold and 63% for sunflower). Patterning of small structures that require e-beam lithography for prototyping can be done using nanoimprint lithography to scale up the patterning area and enable higher throughput [54].

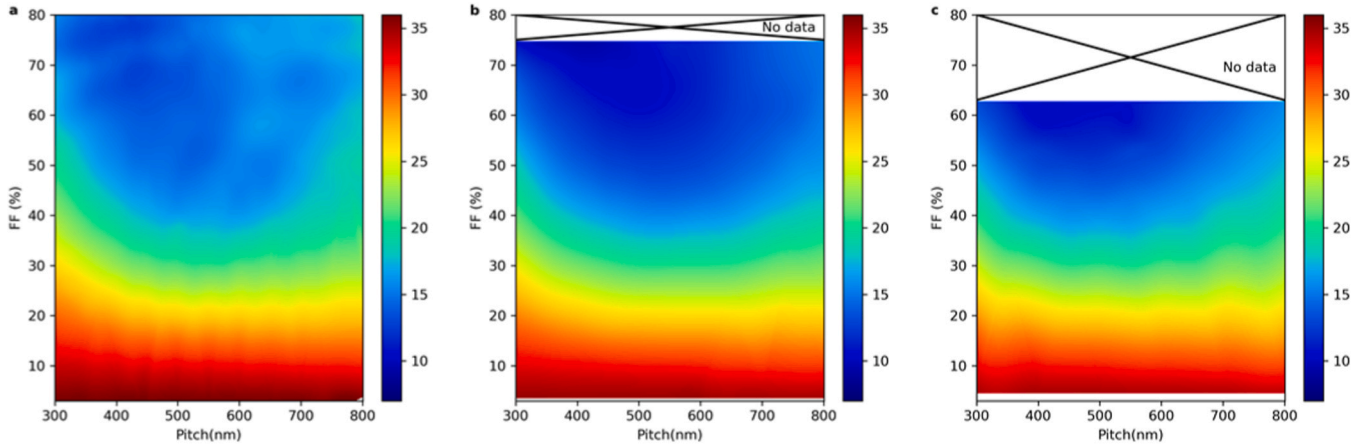

Fig. 5. EAR calculated from simulated reflectance spectra for depth of 1000 nm with lattice pitch and FF being varied for lattice types (a) triangular, (b) 12 fold and (c) sunflower.

Table 1
Comparison of PQC EAR performance to typical AR schemes.

AR scheme	EAR (%)	Reference
Bare Si	36.69	OPAL2 [53]
SLAC 85 nm SiNx	11.36	OPAL2 [53]
Random pyramids	10.96	OPAL2 [53]
Best sunflower for depth 1000 nm	10.1	This work
Best 12 fold for depth 1000 nm	9.2	This work
Random pyramids with 80 SiNx SLAC	2.3	OPAL2 [53]

3.4. Physical mechanisms responsible for performance enhancement

Fig. 6 shows simulated reflectance spectra (as opposed to EAR) for PhCs/PQCs with a fixed lattice pitch of 500 nm and a hole depth of 1000 nm as a function of FF.

As mentioned in the introduction, periodic refractive index modulation provided by PhCs creates 'photon dispersion bands' (akin to electronic dispersion bands in semiconductor materials) each of which provide an optical transmission/leakage path from the external world to trapped modes in the silicon solar cell. Hence dispersion bands couple light to multiple trapped modes associated with the thick silicon solar cell. PQCs have a far higher density of dispersion bands, providing a higher density of optical states than regular PhCs and so are able to trap more light, more efficiently, than conventional triangular and square PhC lattice arrangements.

PhC dispersion features manifest themselves in the data as sharp near-vertical features in the reflectivity plots. These are particularly evident as 'fine texture' in the blue regions of the triangular lattice plot (450–600 nm and FF 30–70%). Since geometric parameters of the PhC/PQCs directly affect the dispersion bands, small changes in lattice parameters can have a significant effect on how the light couples into the Si. Optimizing the geometry therefore allows efficient photon management.

We observe that for very small FF (< 10%) spectral reflectivity converges to the same EAR value as an un-patterned Si surface irrespective of lattice type, suggesting that the PhC has virtually no interaction with incident light. Deviations from the bare Si reflection spectra become significant when FF is larger than 25%. For small FF it is entirely likely that the etched structure simply acts as a reduced refractive index medium, effectively acting as an AR coating, in which case conventional refraction and Fresnel reflection processes dominate.

The situation is very different for high-symmetry PQCs whereby a densely packed continuum of dispersion modes provides a high density of optical states, into which light can couple and consequently very efficient light transmission across the PQC lattice. Incidentally, utilization of dense PhC transmission modes in this way is in complete contrast to most other PhC applications whereby strong light reflection is ensured by total lack of dispersive modes within the photonic band gap. Furthermore, in this configuration light propagates along the length of the holes perpendicular to the plane of the patterning (equivalent to the gamma point on a photonic band diagram).

3.5. Comparisons to effective medium model

To investigate the effective index medium hypothesis in detail, FDTD PhC/PQC simulations compared against an effective medium AR coating model (Fig. 6d), whereby the etched layer is considered as a homogenous material of reduced refractive index (see Section 2 for full detail).

Fig. 6d exhibits clear Fabry Perot (FP) interference fringes (diagonal features) due to destructive/constructive interference within the top layer [55,56]. Two broad diagonal FP fringes are evident for the triangular lattice pitch > 600 nm, modulated by vertical dispersion features. However, FP fringes are entirely absent for the PQC lattices.

Fig. 6e compares reflectance spectra for example devices with identical lattice parameters but different lattice symmetry/type. The triangular lattice clearly shows FP interference fringes for wavelength > 600 nm, but has a pronounced dip over range 450–550 nm, hence it seems that for this design two modes of operation (PhC/effective medium) switch over at 600 nm. 12 fold symmetry PQC lattice follows the same trend closely but does not exhibit the large modulations above 600 nm (but they are weakly evident). We conclude that reduced amplitude of the FP modulation over the long wavelength range significantly improves overall EAR for this lattice. The infinite symmetry sunflower lattice has a very smooth plot, with no clear band gap region or FP fringes. It seems there may be a broad but weak band gap between 500 and 750 nm. Apart from the band gap region it mostly follows the same trend as the lower symmetry lattices. Overall Fig. 6e gives insight into the physical process of operation for the different lattice types.

Fig. 7a plots EAR for similar devices to Fig. 6e (500 nm lattice pitch and 1000 nm hole depth) but in this case over a range of FF (hole diameters). Effective medium simulation is also superimposed.

We observe a near-linear relationship between EAR and FF for all lattice types over FFs range 10–45%. For the effective medium model, a linear relationship largely holds true for the entire FF range, whereas the behavior of the nanostructured surfaces deviates significantly for FF > 50%. As discussed in the previous section, spectral reflectance for PhCs with FF < 10%, behave almost identically to a bare Si surface. Hence results for all lattice types converge to the same value.

Curves for triangular lattice type flattens off when FF > 45% with little further reduction in reflectance. However, EAR values for the PQC lattices continue to show significant reduction in reflectance. Overall,

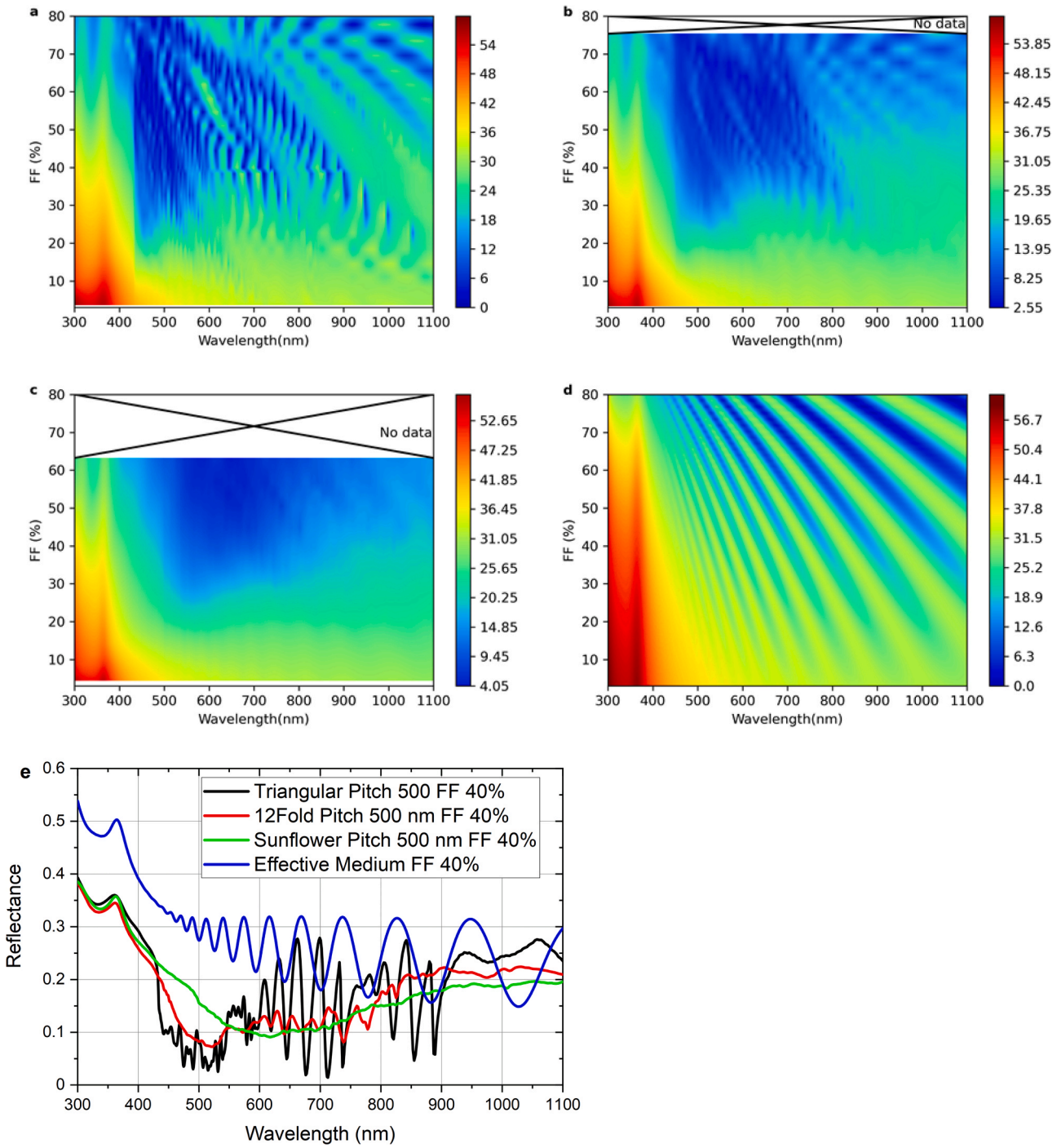

Fig. 6. Reflectance spectra of different lattice types for a lattice pitch of 500 nm and a hole depth of 1000 nm: (a–d) overview contour plots for increasing FF for (a) triangular, (b) 12 fold, (c) sunflower as well as (d) effective medium comparison, (e) comparison of reflectance spectra of different lattice types for same geometrical parameters of lattice pitch 500 nm, FF 40% and depth of 1000 nm.

it's clear that high-symmetry PQC structures provide greatly enhanced EAR performance compared to the low symmetry triangular PhC structures.

3.6. Optimization of hole depth

Having determined physical mechanisms of operation, as well as optimal PhC/PQC design parameters for each lattice type, we now investigate effect of etch depth on EAR performance. Fig. 7b plots EAR as function of hole depth for optimal pitch/FF combinations for each lattice type. Again, effective medium model is included as a baseline comparison.

We observe a sharp reduction in EAR for all PhC lattice types over etch depth range 0–100 nm. A clear dip is visible at 75 nm depth in the case of the effective medium material. This is typical behavior for a single layer AR coating (SLAC). Both the triangular and 12 fold lattice types show a similar dip in reflectance around 100–150 nm hole depth. The effective medium model stabilizes to a minimum EAR of 16% when hole depth $>$ 350 nm. The triangular lattice follows a very similar trend to the effective medium model with increasing hole-depth, exhibiting clear ripples relating to FP fringes at identical hole depth. This further confirms that the triangular PhC lattice predominantly behaves as a

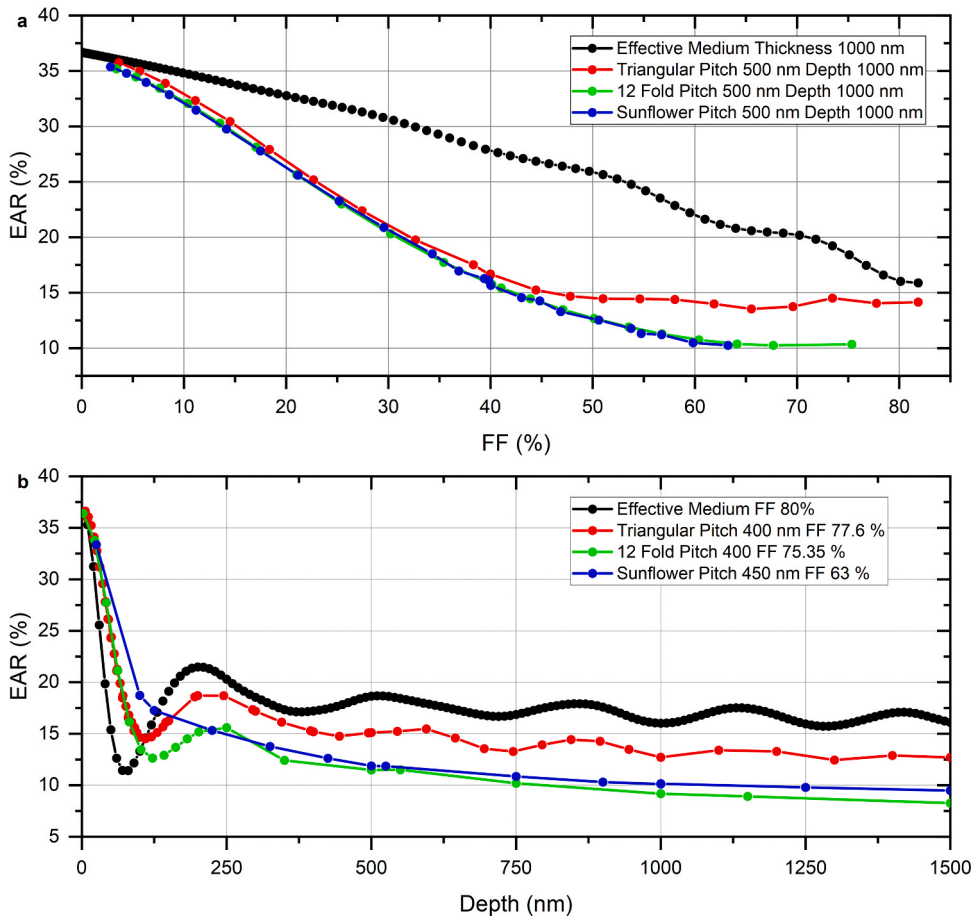

Fig. 7. EAR values for parameter scans, (a) EAR over FF for structures of different lattice type with a lattice pitch of 500 nm and a hole depth of 1000 nm, (b) EAR for a range of depths for best design for each lattice type and effective medium comparison.

reduced refractive index medium under vertical illumination conditions.

The 12 fold PQC has quite different characteristics, suddenly changing behavior when hole depth reaches 350–400 nm. This appears to be the critical depth at which the structure transitions from behaving as an effective index medium to a diffractive PhC structure. EAR for 12 fold and sunflower lattice reduces smoothly as etch depth increases further. The sunflower type lattice behaves quite differently overall with a smooth continuous reduction in EAR with increasing hole depth.

In summary, it's now clear that the PQC lattices behave very differently to the effective index medium model. Deep air holes are found to yield lower overall reflectance values, but with diminishing returns beyond 1000 nm. 12 fold symmetric PQC lattice gives the lowest overall reflectance, achieving 9.2% EAR at 1000 nm depth in comparison to 8.3% for 1500 nm depth (1% point improvement for 500 nm extra hole depth). Very shallow (300 nm deep) holes reduces reflectance to just 12.5% compared to 18% for an equivalent AR coating (30% improvement). This is a promising result since holes deeper than 1000 nm are very challenging to fabricate.

3.7. Other design constraints

PhC/PQC surface texturing inevitably results in a greatly increased surface area due to the large internal surface area of the holes. This could impair electrical properties of a solar cell due to counter-productive surface recombination effects. Surface passivation strategies must therefore be employed to mitigate this problem. Since fabrication of very deep holes is challenging, and excess surface area is to be avoided, sunflower lattice PQC with 500 nm hole depth provides a good practical compromise.

Charge carriers generated in the absorber region must also be extracted to electrodes before electron-hole recombination can occur. The extraction problem relates to carrier lifetime and charge carrier mobility, but is effectively mitigated by use of high-lifetime Si in IBC cells.

3.8. Electrical performance

As explained in detail in the methods section, Quokka simulations were performed to determine electrical performance of the optimal PQC design for each lattice type (determined from the previous analysis) assuming a practically achievable etch depth of 500 nm. These designs had EAR values of 11.5% for the 12 fold, 11.9% for the sunflower and 15.1% for the triangular. A standard IBC solar cell model was utilized with the top surface recombination velocity (SRV) scaled by a correction factor equivalent to the increased surface area due to the etched holes [47,48] (correction factors: 5.24, 5.05, 3.96, 1.0 for triangular PhC, 12 fold PQC, sunflower PQC and unpatterned Si respectively).

From Fig. 8a we observe significant increase in J_{SC} as lattice symmetry increases, with an overall boost of 35% for the sunflower lattice compared to a non-patterned silicon surface. We also observe a 2% reduction in V_{OC}. The 12 fold and triangular lattice types show an increase in J_{SC} of 28% and 22%, respectively. As Fig. 8b shows, the overall power conversion efficiency is highest for the sunflower lattice with 21.1%., representing a 32% boost over the unmodified Si surface. The sunflower lattice has a higher power conversion boost than any other lattice because it achieves its low EAR with a lower additional surface area, as is reflected in the lower correction factor for the SRV. The triangular lattice is the worst performing type with an efficiency of

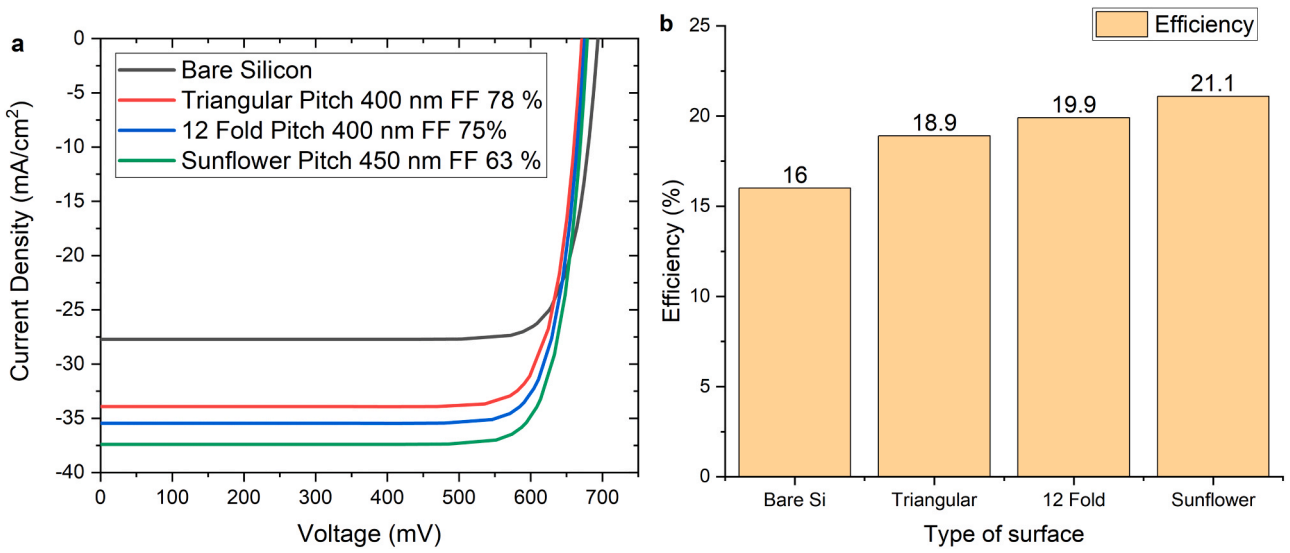

Fig. 8. Results of electrical simulation based on best reflectance results for each lattice type with SRV scaled by surface area: (a) Simulated J-V-curve, (b) extracted parameters of simulated electrical performance.

18.9%. This is due to a combination of improved EAR and reduced additional surface area as lattice symmetry increases. A general trend of increasing efficiency with higher lattice symmetry is observed. Overall, electrical performance is greatly improved compared to a bare silicon surface despite the huge increase in surface area (and associated surface recombination) due to the holes.

4. Conclusion

In summary, after establishing the validity of our simulation setup through comparison to fabricated devices and convergence testing, we rigorously investigated the photon management capabilities of PQC and PhC nanostructuring for Si. We have demonstrated that substantial reductions in top surface reflectance are achievable, with air FF and hole depth emerging as the most important design parameters. For a depth of 1 μm, the 12 fold lattice type yielded the lowest EAR at 9.2% with the sunflower a close second at 10.1%. These low EAR values were shown to be the result of the broad reduction in spectral reflectance seen in the high symmetry PQC lattices. The 6-fold symmetric triangular lattice produced a much less pronounced reduction in reflection, yielding an EAR of 12.5%. The investigation of the physical mechanism behind this reduction showed that PhC type nanostructuring goes beyond a simple effective medium effects offered by random or porous structuring. We've presented a realistic comparison for simulated electrical performance of different lattice types for a realistic etch depth of 500 nm in an IBC solar cell design. Compared to a planar surface, the sunflower lattice emerged as the most promising candidate achieving a 35% boost in J_{sc} and a 32% increase in efficiency this is due to its low EAR of 11.9% for only a modest increase in surface area and thus manageable surface passivation requirements. We conclude that high symmetry PQC structuring offers a novel approach to photon management for next generation Si PV devices.

Funding

This work was supported by the Engineering and Physical Sciences Research Council (EPSRC) via a Ph.D. studentship as well as grants EP/R005303/1 and EP/N00762X/1.

CRediT authorship contribution statement

Thomas M. Mercier: Conceptualization, Methodology, Software, Formal analysis, Investigation, Data curation, Writing - original draft, Visualization. **Dr. Tasmiat Rahman**: Resources, Writing - review & editing, Conceptualization, Software. **Dr. Chirenjeevi Krishnan**: Conceptualization. **Edris Khorani**: Writing - review & editing, Software, Investigation. **Peter J. Shaw**: Data curation, Writing - review & editing. **Dr. Micheal E. Pollard**: Software. **Dr. Stuart A. Boden**: Writing - review & editing, Supervision. **Prof. Pavlos G. Lagoudakis**: Supervision. **Prof. Martin D.B. Charlton**: Writing - review & editing, Supervision, Resources, Project administration.

Declaration of Competing Interest

The authors declare that they have no known competing financial interests or personal relationships that could have appeared to influence the work reported in this paper.

References

[1] N. Taylor, A. Jäger-Waldau, European Commission, Joint Research Centre, Photovoltaics: technology development report, 2019. ⟨https://op.europa.eu/publication/manifestation_identifier/PUB_KJBK19010ENN⟩. (Accessed 15 April 2020).
[2] H. Seigneur, N. Mohajeri, R.P. Brooker, K.O. Davis, E.J. Schneller, N.G. Dhere, M. P. Rodgers, J. Wohlgemuth, N.S. Shiradkar, G. Scardera, A.C. Rudack, W. V. Schoenfeld, Manufacturing metrology for c-Si photovoltaic module reliability and durability, Part I: feedstock, crystallization and wafering, Renew. Sustain. Energy Rev. 59 (2016) 84–106, https://doi.org/10.1016/j.rser.2015.12.343.
[3] N. Asim, K. Sopian, S. Ahmadi, K. Saeedfar, M.A. Alghoul, O. Saadatian, S.H. Zaidi, A review on the role of materials science in solar cells, Renew. Sustain. Energy Rev. 16 (2012) 5834–5847, https://doi.org/10.1016/j.rser.2012.06.004.
[4] L.C. Andreani, A. Bozzola, P. Kowalczewski, M. Liscidini, Photonic light trapping and electrical transport in thin-film silicon solar cells, Sol. Energy Mater. Sol. Cells 135 (2015) 78–92, https://doi.org/10.1016/j.solmat.2014.10.012.
[5] M.S. Branham, W.-C. Hsu, S. Yerci, J. Loomis, S.V. Boriskina, B.R. Hoard, S.E. Han, G. Chen, 15.7% Efficient 10-μm-thick crystalline silicon solar cells using periodic nanostructures, Adv. Mater. 27 (2015) 2182–2188, https://doi.org/10.1002/adma.201405511.
[6] T. Rahman, M. Navarro-Cía, K. Fobelets, High density micro-pyramids with silicon nanowire array for photovoltaic applications, Nanotechnology 25 (2014), 485202, https://doi.org/10.1088/0957-4484/25/48/485202.
[7] S.K. Srivastava, D. Kumar, P.K. Singh, M. Kar, V. Kumar, M. Husain, Excellent antireflection properties of vertical silicon nanowire arrays, Sol. Energy Mater. Sol. Cells 94 (2010) 1506–1511, https://doi.org/10.1016/j.solmat.2010.02.033.
[8] H.K. Raut, V.A. Ganesh, A.S. Nair, S. Ramakrishna, Anti-reflective coatings: a critical, in-depth review, Energy Environ. Sci. 4 (2011) 3779–3804, https://doi.org/10.1039/C1EE01297E.
[9] E. Shi, H. Li, L. Yang, L. Zhang, Z. Li, P. Li, Y. Shang, S. Wu, X. Li, J. Wei, K. Wang, H. Zhu, D. Wu, Y. Fang, A. Cao, Colloidal antireflection coating improves graphene–silicon solar cells, Nano Lett. 13 (2013) 1776–1781, https://doi.org/10.1021/nl400353f.

[10] L. Yu, D.D. Tune, C.J. Shearer, J.G. Shapter, Implementation of antireflection layers for improved efficiency of carbon nanotube–silicon heterojunction solar cells, Sol. Energy 118 (2015) 592–599, https://doi.org/10.1016/j.solener.2015.06.014.

[11] Y. Qian, I. Jeon, Y. Ho, C. Lee, S. Jeong, C. Delacou, S. Seo, A. Anisimov, E. I. Kaupinnen, Y. Matsuo, Y. Kang, H. Lee, D. Kim, J. Delaunay, S. Maruyama, Multifunctional effect of *p* -doping, antireflection, and encapsulation by polymeric acid for high efficiency and stable carbon nanotube-based silicon solar cells, Adv. Energy Mater. 10 (2020), 1902389, https://doi.org/10.1002/aenm.201902389.

[12] J.S. You, D. Kim, J.Y. Huh, H.J. Park, J.J. Pak, C.S. Kang, Experiments on anisotropic etching of Si in TMAH, Sol. Energy Mater. Sol. Cells 66 (2001) 37–44, https://doi.org/10.1016/S0927-0248(00)00156-2.

[13] T. Rahman, R.S. Bonilla, A. Nawabjan, P.R. Wilshaw, S.A. Boden, Passivation of all-angle black surfaces for silicon solar cells, Sol. Energy Mater. Sol. Cells 160 (2017) 444–453, https://doi.org/10.1016/j.solmat.2016.10.044.

[14] Y. Wan, P. Hsiao, W. Zhang, A. Lennon, Y. Chen, Z. Feng, P. Verlinden, C. Samundsett, J. Cui, D. Yan, A. Cuevas, Laser-patterned n-type front-junction silicon solar cell with tantalum oxide/silicon nitride passivation and antireflection, Sol. RRL 2 (2018), 1700187, https://doi.org/10.1002/solr.201700187.

[15] Y.-F. Huang, S. Chattopadhyay, Y.-J. Jen, C.-Y. Peng, T.-A. Liu, Y.-K. Hsu, C.-L. Pan, H.-C. Lo, C.-H. Hsu, Y.-H. Chang, C.-S. Lee, K.-H. Chen, L.-C. Chen, Improved broadband and quasi-omnidirectional anti-reflection properties with biomimetic silicon nanostructures, Nat. Nanotechnol. 2 (2007) 770–774, https://doi.org/10.1038/nnano.2007.389.

[16] H.M. Branz, V.E. Yost, S. Ward, K.M. Jones, B. To, P. Stradins, Nanostructured black silicon and the optical reflectance of graded-density surfaces, Appl. Phys. Lett. 94 (2009), 231121, https://doi.org/10.1063/1.3152244.

[17] H. Savin, P. Repo, G. von Gastrow, P. Ortega, E. Calle, M. Garín, R. Alcubilla, Black silicon solar cells with interdigitated back-contacts achieve 22.1% efficiency, Nat. Nanotechnol. 10 (2015) 624–628, https://doi.org/10.1038/nnano.2015.89.

[18] A. Bozzola, M. Liscidini, L.C. Andreani, Photonic light-trapping versus Lambertian limits in thin film silicon solar cells with 1D and 2D periodic patterns, Opt. Express 20 (2012) A224–A244, https://doi.org/10.1364/OE.20.00A224.

[19] H. Benisty, J.-M. Lourtioz, A. Chelnokov, S. Combrie, X. Checoury, Recent advances toward optical devices in semiconductor-based photonic crystals, Proc. IEEE 94 (2006) 997–1023, https://doi.org/10.1109/JPROC.2006.873441.

[20] T. Ishigaki, M. Fujita, M. Nagai, M. Ashida, T. Nagatsuma, Photonic-crystal slab for terahertz-wave integrated circuits, in: IEEE Photonics Conference 2012, IEEE, Burlingame, CA, USA, 2012, pp. 774–775. https://doi.org/10.1109/IPCon.2012.6358852.

[21] H.C. Nguyen, Y. Sakai, M. Shinkawa, N. Ishikura, T. Baba, Photonic crystal silicon optical modulators: carrier-injection and depletion at 10 Gb/s, IEEE J. Quantum Electron. 48 (2012) 210–220, https://doi.org/10.1109/JQE.2011.2174338.

[22] M. Tillin, M.D.B. Charlton, Z. Gong, A.Z. Khokhar, D. Massoubre, I.M. Watson, E. Gu, M.D. Dawson, F. Rahman, N.P. Johnson, D. Macintyre, R.M.D.L. Rue, K. Parsons, S. Lin, Photonic quasi-crystal light emitting diodes: comparisons of device performance with pattern pitch, in: Photonic Crystal Materials and Devices IX, International Society for Optics and Photonics, 2010, p. 77130B. https://doi.org/10.1117/12.853796.

[23] H.-W. Huang, C.-H. Lin, Z.-K. Huang, K.-Y. Lee, C.-C. Yu, H.-C. Kuo, Double photonic quasi-crystal structure effect on GaN-based vertical-injection light-emitting diodes, Jpn. J. Appl. Phys. 49 (2010), 022101, https://doi.org/10.1143/JJAP.49.022101.

[24] M.D.B. Charlton, P.A. Shields, D.W.E. Allsop, W.N. Wang, High-efficiency photonic quasi-crystal light emitting diodes incorporating buried photonic crystal structures, in: Tenth International Conference on Solid State Lighting, International Society for Optics and Photonics, 2010, p. 778407. https://doi.org/10.1117/12.860585.

[25] P.A. Shields, M.D.B. Charlton, T. Lee, M.E. Zoorob, D.W.E. Allsopp, W.N. Wang, Enhanced light extraction by photonic quasi-crystals in GaN Blue LEDs, IEEE J. Sel. Top. Quantum Electron. 15 (2009) 1269–1274, https://doi.org/10.1109/JSTQE.2009.2016674.

[26] C. Lee, C. Lai, Y. Lee, H. Kuo, T. Lu, S. Wang, Nitride-based thin-film light-emitting diodes with photonic quasi-crystal surface, IEEE Photonics Technol. Lett. 21 (2009) 331–333, https://doi.org/10.1109/LPT.2008.2010953.

[27] T.M. Mercier, C. Krishnan, P.J. Shaw, P.G. Lagoudakis, M.D.B. Charlton, Photonic crystal based control of directionality in GaN based LEDs, in: Light-Emitting Devices, Materials, and Applications XXIV, International Society for Optics and Photonics, 2020, p. 113021P. https://doi.org/10.1117/12.2543124.

[28] P. Bermel, C. Luo, L. Zeng, L.C. Kimerling, J.D. Joannopoulos, Improving thin-film crystalline silicon solar cell efficiencies with photonic crystals, Opt. Express 15 (2007) 16986, https://doi.org/10.1364/OE.15.016986.

[29] Y.-J. Hung, S.-L. Lee, L.A. Coldren, Deep and tapered silicon photonic crystals for achieving anti-reflection and enhanced absorption, Opt. Express 18 (2010) 6841–6852, https://doi.org/10.1364/OE.18.006841.

[30] S.A. Boden, D.M. Bagnall, Nanostructured biomimetic moth-eye arrays in silicon by nanoimprint lithography, in: R.J. Martin-Palma, A. Lakhtakia (Eds.), San Diego, CA, 2009, p. 74010J. https://doi.org/10.1117/12.826201.

[31] A. Asadollahbaik, S.A. Boden, M.D.B. Charlton, D.N.R. Payne, S. Cox, D.M. Bagnall, Reflectance properties of silicon moth-eyes in response to variations in angle of incidence, polarisation and azimuth orientation, Opt. Express 22 (2014) A402–A415, https://doi.org/10.1364/OE.22.00A402.

[32] T. Rahman, K. Fobelets, Efficient tool flow for 3D photovoltaic modelling, Comput. Phys. Commun. 193 (2015) 124–130, https://doi.org/10.1016/j.cpc.2015.03.016.

[33] M.E. Zoorob, M.D.B. Charlton, G.J. Parker, J.J. Baumberg, M.C. Netti, Complete photonic bandgaps in 12-fold symmetric quasicrystals, Nature 404 (2000) 740–743, https://doi.org/10.1038/35008023.

[34] T.D.M. Lee, G.J. Parker, M.E. Zoorob, S.J. Cox, M.D.B. Charlton, Design and simulation of highly symmetric photonic quasi-crystals, Nanotechnology 16 (2005) 2703–2706, https://doi.org/10.1088/0957-4484/16/11/039.

[35] M.D.B. Charlton, M.E. Zoorob, T. Lee, Photonic quasi-crystal LEDs: design, modelling, and optimisation, in: Light Emitting Diodes: Research, Manufacturing, and Applications XI, International Society for Optics and Photonics, 2007, p. 64860R. https://doi.org/10.1117/12.715025.

[36] M.E. Pollard, G.J. Parker, M.D.B. Charlton, Photonic band gaps of increasingly isotropic crystals at high dielectric contrasts, in: Photonic and Phononic Properties of Engineered Nanostructures II, International Society for Optics and Photonics, 2012, p. 82690W. https://doi.org/10.1117/12.908174.

[37] M.E. Pollard, G.J. Parker, Low-contrast bandgaps of a planar parabolic spiral lattice, Opt. Lett. 34 (2009) 2805–2807, https://doi.org/10.1364/OL.34.002805.

[38] M.D.B. Charlton, 10 - Photonic crystal nitride LEDs, in: J. Huang, H.-C. Kuo, S.-C. Shen (Eds.), Nitride Semiconductor Light-Emitting Diodes LEDs, second ed, Woodhead Publishing, 2018, pp. 327–376, https://doi.org/10.1016/B978-0-08-101942-9.00010-1.

[39] T. Rahman, S.A. Boden, Optical modeling of black silicon for solar cells using effective index techniques, IEEE J. Photovolt. 7 (2017) 1556–1562, https://doi.org/10.1109/JPHOTOV.2017.2748900.

[40] A. Prajapati, Y. Nissan, T. Gabay, G. Shalev, Broadband absorption of the solar radiation with surface arrays of subwavelength light funnels, Nano Energy 54 (2018) 447–452, https://doi.org/10.1016/j.nanoen.2018.10.046.

[41] G. Shalev, S.W. Schmitt, G. Brönstrup, S. Christiansen, Maximizing the ultimate absorption efficiency of vertically-aligned semiconductor nanowire arrays with wires of a low absorption cross-section, Nano Energy 12 (2015) 801–809, https://doi.org/10.1016/j.nanoen.2015.01.048.

[42] Nanophotonic FDTD Simulation Software - Lumerical FDTD, Lumerical. (n.d.). ⟨https://www.lumerical.com/products/fdtd/⟩. (Accessed 27 January 2020).

[43] M. Oxborrow, C.L. Henley, Random square-triangle tilings: a model for twelvefold-symmetric quasicrystals, Phys. Rev. B 48 (1993) 6966–6998, https://doi.org/10.1103/PhysRevB.48.6966.

[44] H. Vogel, A better way to construct the sunflower head, Math. Biosci. 44 (1979) 179–189, https://doi.org/10.1016/0025-5564(79)90080-4.

[45] J.A. de Río, S. Whitaker, Maxwell's equations in two-phase systems i: local electrodynamic equilibrium, Transp. Porous Media 39 (2000) 159–186, https://doi.org/10.1023/A:1006617029519.

[46] F. Zhan, Z. Li, X. Shen, H. He, J. Zeng, Design multilayer antireflection coatings for terrestrial solar cells, Sci. World J. 2014 (2014) 1–5, https://doi.org/10.1155/2014/265351.

[47] A. Fell, K.C. Fong, K.R. McIntosh, E. Franklin, A.W. Blakers, 3-D simulation of interdigitated-back-contact silicon solar cells With Quokka including perimeter losses, IEEE J. Photovolt. 4 (2014) 1040–1045, https://doi.org/10.1109/JPHOTOV.2014.2320302.

[48] A. Fell, A free and fast three-dimensional/two-dimensional solar cell simulator featuring conductive boundary and quasi-neutrality approximations, IEEE Trans. Electron Devices 60 (2013) 733–738, https://doi.org/10.1109/TED.2012.2231415.

[49] Franklin Evan, Fong Kean, Mc.Intosh Keith, Fell Andreas, Blakers Andrew, Kho Teng, Walter Daniel, Wang Da, Zin Ngwe, Stocks Matthew, Wang Er-Chien, Grant Nicholas, Wan Yimao, Yang Yang, Zhang Xueling, Feng Zhiqiang, J. Verlinden Pierre, Design, fabrication and characterisation of a 24.4% efficient interdigitated back contact solar cell, Prog. Photovolt. Res. Appl. 24 (2014) 411–427, https://doi.org/10.1002/pip.2556.

[50] A. Fell, K.R. McIntosh, P.P. Altermatt, G.J.M. Janssen, R. Stangl, A. Ho-Baillie, H. Steinkemper, J. Greulich, M. Müller, B. Min, K.C. Fong, M. Hermle, I.G. Romijn, M.D. Abbott, Input parameters for the simulation of silicon solar cells in 2014, IEEE J. Photovolt. 5 (2015) 1250–1263, https://doi.org/10.1109/JPHOTOV.2015.2430016.

[51] G. Dingemans, W.M.M. Kessels, Status and prospects of Al2O3-based surface passivation schemes for silicon solar cells, J. Vac. Sci. Technol. A Vac. Surf. Films 30 (2012), 040802, https://doi.org/10.1116/1.4728205.

[52] M.D.B. Charlton, S.W. Roberts, G.J. Parker, Guided mode analysis, and fabrication of a 2-dimensional visible photonic band structure confined within a planar semiconductor waveguide, Mater. Sci. Eng. B 49 (1997) 155–165, https://doi.org/10.1016/S0921-5107(97)00102-5.

[53] K.R. McIntosh, S.C. Baker-Finch, OPAL 2: Rapid optical simulation of silicon solar cells, in: 2012 38th IEEE Photovoltaic Specialists Conference, 2012, pp. 000265–000271. https://doi.org/10.1109/PVSC.2012.6317616.

[54] B.S. Cheng, C.H. Chiu, K.J. Huang, C.F. Lai, H.C. Kuo, C.H. Lin, T.C. Lu, S.C. Wang, C.C. Yu, Enhance light extraction of InGaN-based green LEDs by nano-imprinted 2D photonic crystal pattern, Semicond. Sci. Technol. 23 (2008), 055002, https://doi.org/10.1088/0268-1242/23/5/055002.

[55] E. Hecht, Optics, Pearson, Harlow, England, 2014. Accessed 27 August 2020, ⟨http://www.myilibrary.com?id=527420⟩.

[56] Q. Yang, X.A. Zhang, A. Bagal, W. Guo, C.-H. Chang, Antireflection effects at nanostructured material interfaces and the suppression of thin-film interference, Nanotechnology 24 (2013), 235202, https://doi.org/10.1088/0957-4484/24/23/235202.

Thomas Manuel Mercier Thomas completed his BSc in Nanoegineering at the University of Duisburg-Essen in Germany, which was followed by completing an MSc in Nanoelectronics at the University of Southampton in the UK, where he is currently working on a PhD in using colloidal Quantum Dots and Photonic Quasi Crystals in Si PV and GaN based LEDs. He is also currently employed as a senior research assistant working on Si/Lithium Niobate based modulators.

Dr Tasmiat Rahman is a Lecturer in the School of Electronics and Computer Science (ECS) at the University of Southampton. He graduated from Imperial College London in 2011, with a first-class honours degree in Electrical and Electronic Engineering, and then awarded a PhD in 2016, for his work on light trapping nano-structures for silicon photovoltaics. He then joined ECS as a post-doctoral researcher, working on tandem-cell architectures and quantum materials. He was promoted to Senior Research Fellow in 2018, where he worked on black silicon surfaces for industrial photovoltaics. Tasmiat was appointed as a lecturer for ECS in 2021.

Dr Chirenjeevi Krishnan received his MSc in Nanoelectronics and PhD Degree in Electronics and Electrical engineering from the University of Southampton, UK in 2010 and 2016 respectively. His doctor and postdoctoral work were on hybrid optoelectronic devices. His research interests are photonic crystals, VCSELs, Nanofabrication, Quantum Dots, Hybrid LEDs and solar cells. As of 2020, he is working on his health tech start-up and consulting on agrophotovoltaics.

Edris Khorani completed his BEng in Electronic Engineering in 2016 at the University of Southampton. This was followed by the completion of his Ph.D. in hole-selective passivating contacts for silicon solar cells in 2021, supported by the Centre for Doctoral Training: New and Sustainable Photovoltaics (CDT-PV).

Peter J. Shaw Peter completed his MPhys in Physics with Nanotechnology at the University of Southampton, UK, where he remained to finish work on his PhD in Electronic Engineering focusing on the synthesis and properties of quantum dots.

Dr. Michael Pollard Michael received his BEng in Electronic Engineering and PhD in Nanophotonics from the University of Southampton in 2006 and 2011, respectively, and was awarded the Sir William Siemens Medal. His doctoral thesis focused on manipulating the transmission and emission of light using photonic crystals. This expertise resulted in a 3-year appointment to a multi-disciplinary EU FP7 project (PHOTOSENS) developing photonic crystal-based biosensors. As part of this work, he also developed scientific instruments for measurement of luminescence and light scattering. In 2014, he joined UNSW Sydney as a Research Fellow within the School of Photovoltaic and Renewable Energy Engineering.

Dr. Stuart Boden is an Associate Professor in the School of Electronics and Computer Science at the University of Southampton, UK. He graduated with an MEng in Materials Science from the University of Oxford in 2004 and received his PhD in Electronics and Electrical Engineering from the University of Southampton in 2009 for his work on the development of nanostructured antireflective surfaces for photovoltaics. His current research focuses on antireflection and light trapping schemes for crystalline silicon photovoltaics. He has authored or co-authored over 40 journal articles, over 40 conference articles and 5 book chapters.

Prof. Pavlos Lagoudakis Graduate of the University of Athens, Greece, Professor Pavlos Lagoudakis received his PhD degree in Physics from the University of Southampton, UK in 2003 and conducted his postdoctoral research on optoelectronic properties of organic semiconductors at the Ludwig Maximilians University of Munich, Germany. In 2006, he returned to Southampton as Lecturer at the department of Physics and Astronomy, where he set up a new experimental activity on Hybrid Photonics. In 2016, Prof Pavlos Lagoudakis setup and directs the Hybrid Photonics Labs at Skoltech, Moscow, a photonics foundry dedicated to the physics and applications of liquid light.

Prof. Martin D. B. Charlton is professor of nano-photonics, and nano-fabrication at the at the University of Southampton UK. He held a 'Royal Society Research Fellowship' for 10 years, was awarded the "Rank phd thesis prize" in 1999, and founded Mesophotonics ltd in 2001. His research interests include: Diffractive Optics, directional VCSELs and LEDs, Hybrid LEDs and Photovoltaics and Micro-Displays. He holds 33 granted patents in the field of photonic quasi-crystals, has over 200 academic publications and holds visiting Professor positions at JAIST (Japan) and Xian Jiatong University (China).